



U.S. DEPARTMENT OF  
**ENERGY**

Office of  
Science

DOE/SC-ARM/TR-133

# **Aerosol Optical Depth Value-Added Product for the SAS-He Instrument**

B Ermold  
CJ Flynn  
J Barnard

September 2013  
Version 1.0



## **DISCLAIMER**

This report was prepared as an account of work sponsored by the U.S. Government. Neither the United States nor any agency thereof, nor any of their employees, makes any warranty, express or implied, or assumes any legal liability or responsibility for the accuracy, completeness, or usefulness of any information, apparatus, product, or process disclosed, or represents that its use would not infringe privately owned rights. Reference herein to any specific commercial product, process, or service by trade name, trademark, manufacturer, or otherwise, does not necessarily constitute or imply its endorsement, recommendation, or favoring by the U.S. Government or any agency thereof. The views and opinions of authors expressed herein do not necessarily state or reflect those of the U.S. Government or any agency thereof.

# **Aerosol Optical Depth Value-Added Product for the SAS-He Instrument**

B Ermold  
CJ Flynn  
J Barnard

September 2013  
Version 1.0

Work supported by the U.S. Department of Energy,  
Office of Science, Office of Biological and Environmental Research

## Contents

1.0	Introduction .....	1
2.0	Description of Algorithm.....	2
2.1	Overview.....	2
2.2	Langley Retrievals.....	2
2.3	Obtaining Robust Daily Calibrations.....	8
2.4	Computing Total and Aerosol Optical Depths.....	10
2.5	Aerosol Optical Depths – An Example .....	13
2.6	Application of a Cloud Screen.....	14
3.0	Algorithm Technical Considerations.....	15
3.1	Change of Hardware or Unexpected Data Gaps .....	15
3.2	VAP Output .....	15
3.3	Running the SAS-He Langley and AOD VAPs (command line arguments).....	15
3.4	Data Quality Assessment Included .....	16
3.5	Known Issues.....	17
4.0	References .....	18
	Appendix A Table of wavelength versus ozone absorption coefficients.....	A.1
	Appendix B Contents of netCDF output for the SAS-He Langley VAP.....	B.1
	Appendix C Contents of netCDF output for the SAS-He AOD VAP .....	C.1

## Figures

1.	Illustration of a Langley regression. ....	4
2.	Multiple Langley regressions.....	5
3.	Retrieved $I_o$ values for all pixels from the Si CCD array within the VIS spectrometer design wavelength range.....	6
4.	Retrieved $I_o$ values for all pixels from the InGaAs linear array within the NIR spectrometer design wavelength range .....	7
5.	Variability of the retrieved $I_o$ values after interquartile filtering normalized to the mean and multiplied by 100 to convert to percent. ....	8
6.	Time series of $I_o$ values (blue dots) from the SAS-He at the ARM PVC site.....	9
7.	TOD spectrum with the Rayleigh component removed.....	11
8.	Same as Figure 7 except for the near-IR region extending from about 900 to 1750 nm. ....	12
9.	Time series of AOD for 500 nm wavelength for April 1, 2013 at the ARM PVC site.....	14

## **Tables**

1.	Corrections for gaseous absorption for two selected wavelengths in the near-IR. ....	13
2.	.....	A.1
3.	.....	B.1
4.	.....	C.1

## 1.0 Introduction

The Shortwave Array Spectroradiometer – Hemispheric (SAS-He) is a ground-based, shadowband instrument that measures the direct and diffuse solar irradiance. In this regard, the instrument is similar to the Multi-Filter Rotating Shadowband Radiometer (MFRSR) – an instrument that has been in the ARM suite of instruments for more than 15 years. However, the two instruments differ significantly in wavelength resolution and range. In particular, the MFRSR only observes the spectrum in six discrete wavelength channels of about 10 nm width from 415 to 940 nm. The SAS-He, in contrast, incorporates two fiber-coupled grating spectrometers: a Si CCD spectrometer with over 2000 pixels covering the range from 325-1040 nm with ~ 2.5 nm resolution, and an InGaAs array spectrometer with 256 pixels covering the wavelength range from 960-1700 nm with ~ 6 nm resolution.

The irradiances measured by the SAS-He form the basis of deriving aerosol optical depth (AOD)—a quantity that is critical for understanding atmospheric radiative transfer and its effect on climate. This document describes the process applied to retrieve AOD from the SAS-He measurements. Because the processing path leading from measurements of direct normal irradiance to AOD is nearly identical for the MFRSR and the SAS-He, this document will closely parallel a similar document written for the MFRSR (Koontz et al., 2013). This document describes two ARM “Value-Added Products” (VAPs) related to the SAS-He. The first of these is the VAP “SAS-He Langley”, which operates on a daily basis to compute Langley regressions from SAS-He measurement data. The second VAP, called “SAS-He AOD”, first processes a multi-week collection of SAS-He Langley results to yield robust daily calibrations, and then applies these daily calibrations to SAS-He direct normal irradiance to retrieve total column optical depth and cloud-screened AOD when line of sight to the sun is unobstructed. The processes in these two VAPs include:

- routine “autonomous” (i.e., capable of being run with minimal human intervention) computation of Langley retrievals that yield first-order “ $I_o$ ” calibration data (“ $I_o$ ” is an estimate of the top-of-atmosphere irradiance, described below),
- generation of a robust time series of smoothed filtered  $I_{o,f}$  from these first-order  $I_o$  values,
- using these  $I_{o,f}$  values, retrieval of optical depth in appropriate SAS-He wavelength ranges, and
- final application of an autonomous cloud screen to the AODs.

The autonomous Langley retrievals have been described in Harrison and Michalsky (1994). The generation of the robust calibration time series combines some of the techniques described in Michalsky et al. (2001), as well as operational elements unique to the ARM deployments, to be detailed below. The cloud screen algorithm is described in Alexandrov et al. (2004).

In addition, we will describe related inputs, the breadth of the VAP outputs, and options for execution.

## 2.0 Description of Algorithm

### 2.1 Overview

The core purpose of the Atmospheric Radiation Measurements program is to reduce uncertainties in climate model predictions. A dominant source of uncertainty in these models is the radiative impact of aerosols, which has spawned a major effort in ARM to measure aerosol properties. The two VAPs described here are concerned with an important radiatively significant aerosol optical property, the AOD. The AOD is a measure of the total aerosol burden in the atmosphere, and direct aerosol radiative forcing is strongly influenced by this quantity.

The determination of AODs from the SAS-He depends on in-field calibration with Langley regressions, which are linear regressions of the log of the measured irradiance versus airmass, computed on a twice-daily basis. Given the output of these regressions, it is possible to field calibrate the SAS-He. However, the daily Langley regressions exhibit significant noise due mostly to atmospheric variability. The SAS-He Langley VAP requires several weeks of operational measurements to accumulate enough acceptable Langley regressions to reduce statistical variability below 1% per day. After applying a stable daily calibration to the radiometric measurements, time series of total optical depths are calculated for each wavelength of the SAS-He. The AOD is then computed as the residual of the total optical depth minus the pressure-corrected Rayleigh optical depth and, if needed, optical depths attributable to absorption from gases including ozone, water vapor, carbon dioxide (CO<sub>2</sub>), nitrogen dioxide (NO<sub>2</sub>), and methane (CH<sub>4</sub>). Lastly, the resulting AODs are flagged to indicate cloud contamination on failure of a variability screen or when direct slant-path transmittance is less than 1%.

### 2.2 Langley Retrievals

Here we review the basics of the Langley regression. At a given wavelength  $\lambda$  with no clouds between the sun and the earth's surface, the un-calibrated direct normal irradiance at the surface  $I(\lambda)$  may be described as:

$$I(\lambda) = I_0(\lambda) \exp[-(\tau_{\text{Rayleigh}} + \tau_{\text{aerosol}})am - \tau_{\text{gas}}(am)] \quad (1)$$

where  $I_0(\lambda)$  is the top-of-atmosphere irradiance (known colloquially as “I-naught”) with units of “counts”,  $am$  is the airmass,  $\tau_{\text{gas}}(am)$  is the gaseous absorption as a function of airmass,  $\tau_{\text{Rayleigh}}$  is the Rayleigh optical depth due to molecular scattering, and  $\tau_{\text{aerosol}}$  is the AOD. Note that the airmass is a time-varying unitless quantity representing the amount of atmosphere in a line of sight between the sun and the surface, normalized equal to one when the sun is directly overhead. Given the time of day, and the site's latitude and longitude, the airmass is calculated using the formula of Kasten and Young (1989):

$$am = 1.0 / [\cos(Z) + 0.50572 \times (96.07995 - Z)^{-1.6364}] \quad (2)$$

where  $Z$  is the solar zenith angle. This formulation of airmass includes corrections for a spherical earth and atmosphere, and for atmospheric refraction.

For many, but not all, parts of the solar spectrum, gaseous absorption is either negligible or linearly proportional to the airmass. For these spectral regions, the above equation becomes:

$$I(\lambda) = I_0(\lambda) \exp[-(\tau_{Rayleigh} + \tau_{aerosol} + \tau_{gas})am] \quad (3)$$

Taking the natural logarithm of each side gives:

$$\ln[I(\lambda)] = \ln[I_0(\lambda)] - (\tau_{Rayleigh} + \tau_{aerosol} + \tau_{gas})am \quad (4)$$

This equation is the essence of the Langley regression. Under suitably stable conditions the various “ $\tau$ ” optical depth components will be approximately constant and this equation reduces to that of a straight line as a function of  $am$ . The y-intercept “ $\ln[I_0(\lambda)]$ ” is log of the irradiance that the instrument would report for an airmass of zero, *i.e.* at the “top of the atmosphere”. For wavelengths where equation 3 is valid (that is, when  $\tau_{gas}$  is either negligible or linear in airmass), this y-intercept provides the means of calibrating the measurements in a relative sense as atmospheric transmittance  $T(\lambda) = I(\lambda)/I_0(\lambda)$  or alternatively casting irradiance in absolute units by reference to published values for “top-of-atmosphere” or “extraterrestrial” irradiance (Gueymard 2004).

The SAS-He Langley VAP produces, at most, one  $I_o$  value for each of two distinct time periods during daylight hours. The first period is for morning hours, for airmass values between 3 and 1; the second period is for afternoon hours for airmass values between 1 and 3. Each Langley regression is deemed “good” or “bad”. A substantial cause of a poor Langley regression is cloud contamination. The algorithm attempts to remove cloud contaminated measurements by iteratively computing a Langley regression, discarding outliers that fall more than two standard deviations from the regression line, and re-computing the regression until either no points are rejected or less than half the original points remain. Because clouds are expected to affect all of the measured wavelengths at a given time, this initial cloud rejection is determined from only a single wavelength chosen at 500 nm where signal levels are typically optimal, but is then applied as a mask to exclude measurements at those times for all measured wavelengths. In addition, a wavelength dependent mask is applied to further restrict the airmass range for those wavelengths with relatively low detection sensitivity. Typical results of this iterative outlier rejection scheme are illustrated for measurements at 500 nm in Figure 1. Figure 2 shows the corresponding results when this same mask is applied to measurements at a selection of five wavelengths corresponding to MFRSR detection wavelengths. Extending the Langley calibration to the full pixel range of both spectrometers yields figures 3 and 4 for the silicon CCD and InGaAs array detectors, respectively. Instead of only a handful of carefully selected discrete channels, the calibration of each spectrometer represents a “spectrum” of  $I_o$  values over the entire wavelength range.

However, it should be noted that these  $I_o$  values in figures 3 and 4 are implicitly valid only at those wavelengths where gaseous absorption is either negligible or is linear in airmass as required by Equation 3. For example, Figure 5 shows the percent variability of a collection of 30  $I_o$  spectra from both the Si CCD and InGaAs array spectrometers. Different colored symbols identify different trace gas constituents or other potential erroneous contributions. The several identifiable structures represent the presence of gas absorption and indicate that these raw retrieved  $I_o$  values can be inaccurate by as much as a factor of two. This will be addressed through subsequent efforts through lamp calibrations (Schmid et al. 1995, Kiedron et al. 1999) to determine the responsivity where gas absorption is strong and/or through “modified Langley” retrievals (Schmid et al. 2001) in which the nonlinear dependence on airmass is explicitly accounted for.

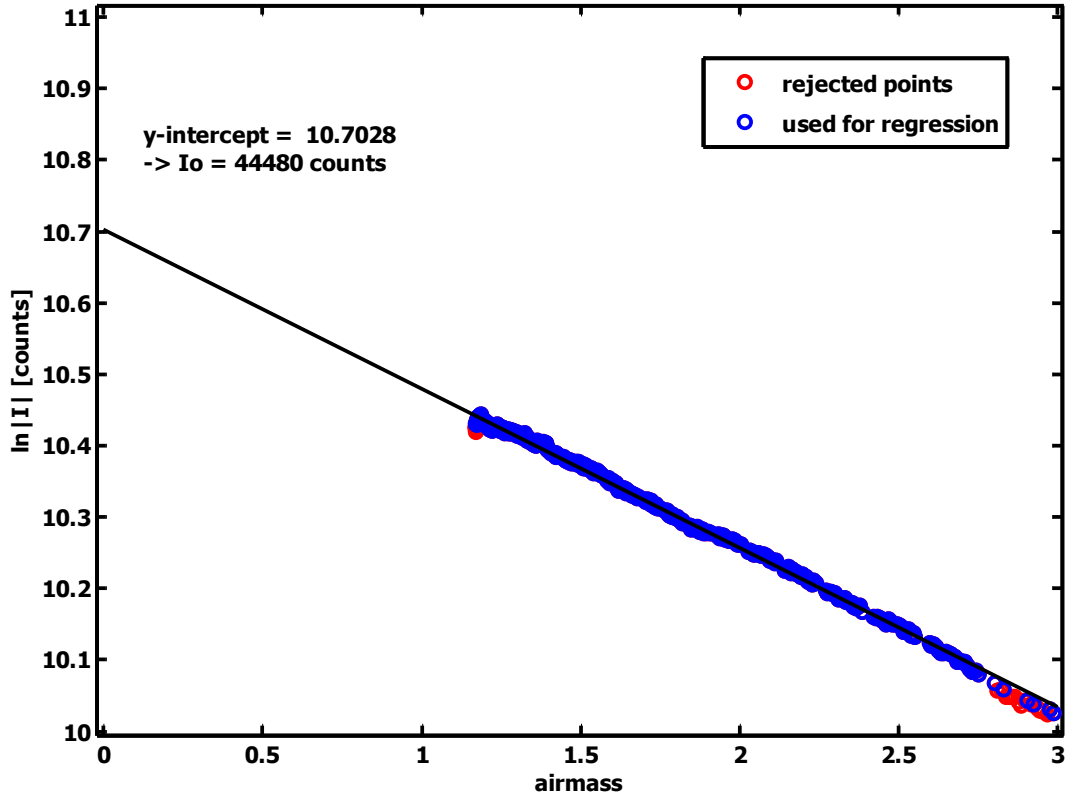


**Figure 1.** Illustration of a Langley regression. The data for this regression, represented by the blue dots, is taken from the PVC TCAP SAS-He on April 17, 2013, in the afternoon. The wavelength is 500 nm. The black line indicates a linear fit to these data. The y-intercept is  $\ln[I_0(\lambda)]$  implying a “top-of-atmosphere”  $I_0$  value of about 44,500 counts. The red dots represent data that is rejected by the algorithm; this rejection may be due to cloud contamination.

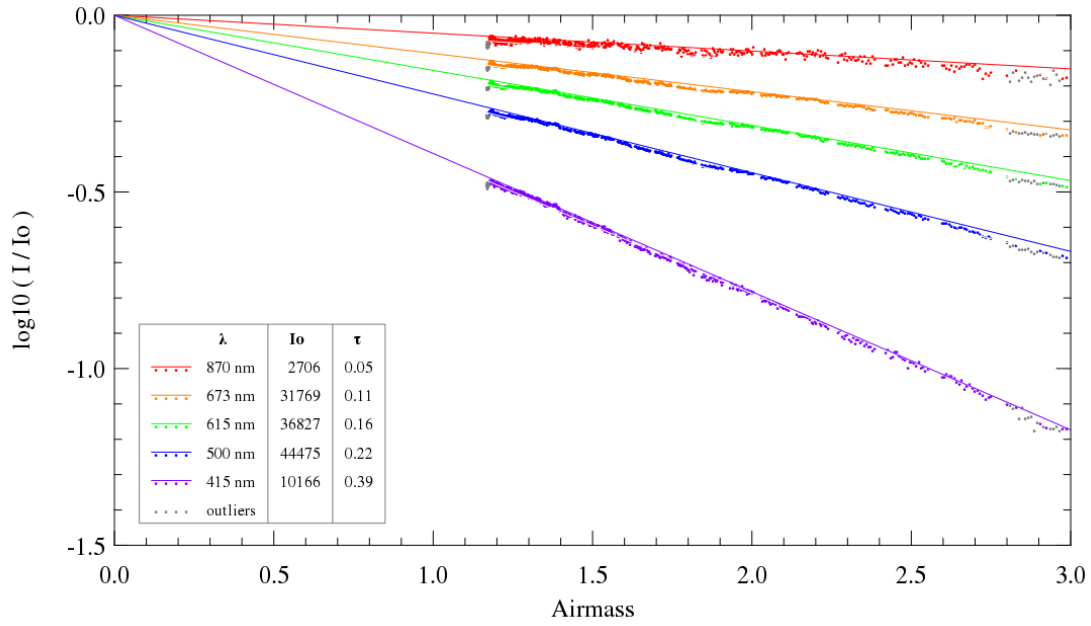


**Figure 2.** Multiple Langley regressions. Langley regressions are shown here are for several selected SAS-He wavelengths comparable to MFRSR filter wavelengths, with the outlier rejection mask determined iteratively at 500 nm applied to all wavelengths. The measurements at each wavelength have been normalized against their respective  $I_0$  values so that each yields a y-intercept of unity while the decreasing optical depth as function of wavelength is evident in the monotonic decrease in slope of the regression lines as a function of wavelength.

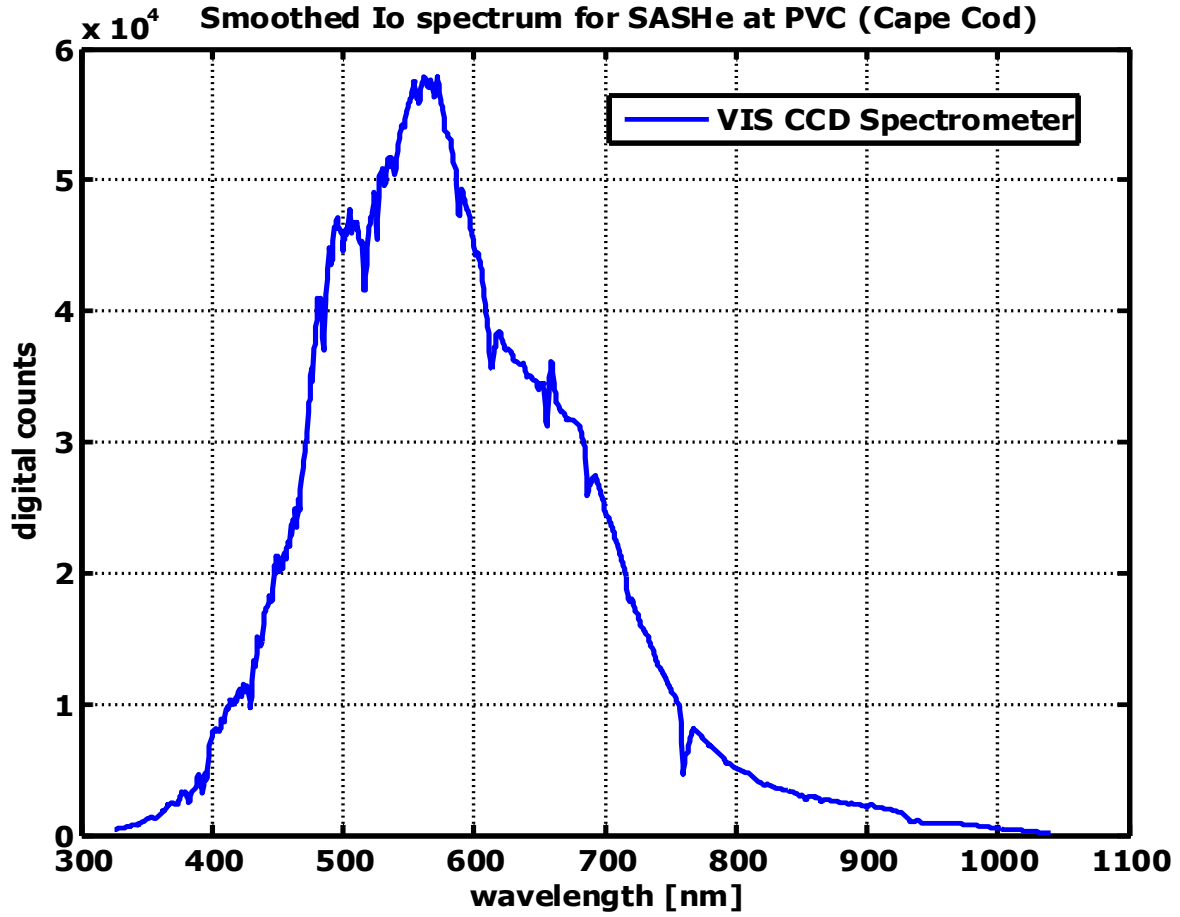


**Figure 3.** Retrieved  $I_0$  values for all pixels from the Si CCD array within the VIS spectrometer design wavelength range. Note that strictly speaking many of these retrieved values are invalid due to the potential effects of gas phase absorption. This will be treated more rigorously later as referenced at the end of Section 2.2.

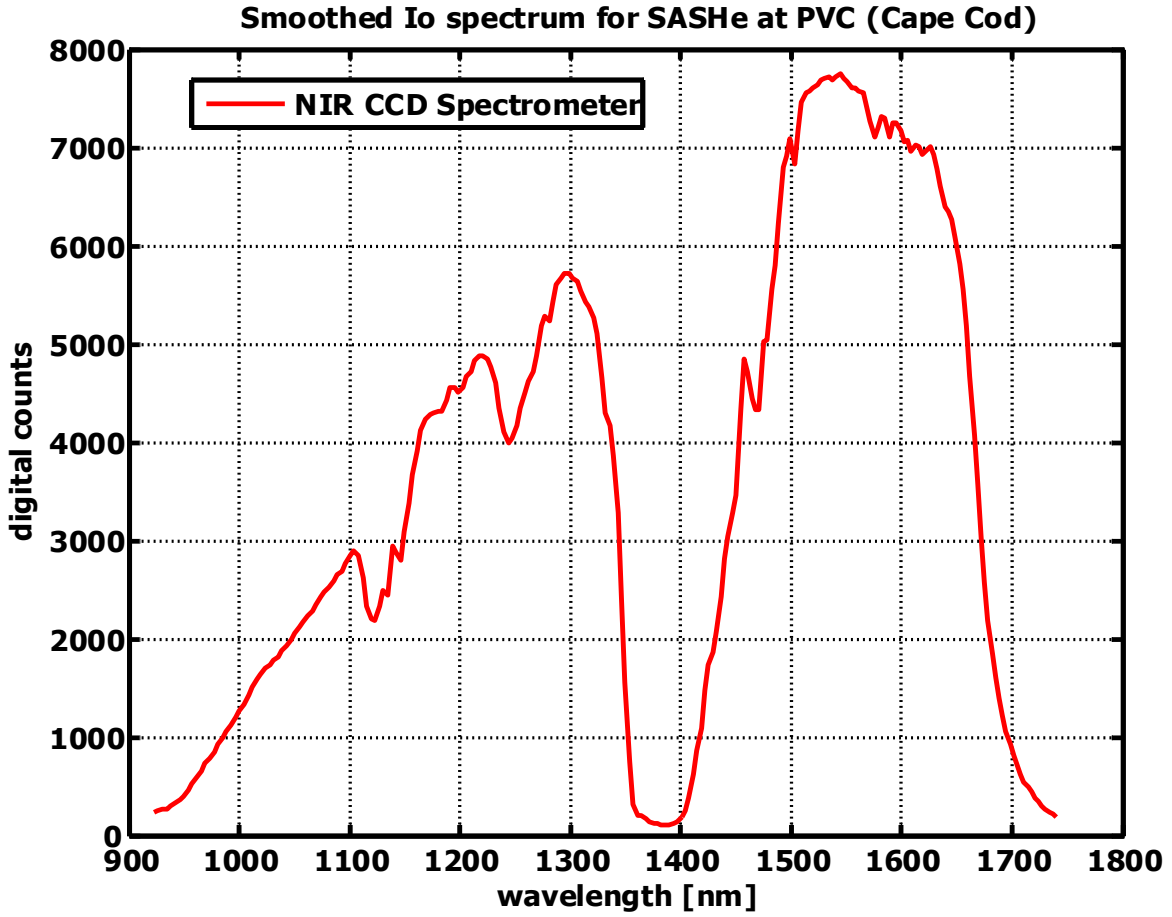
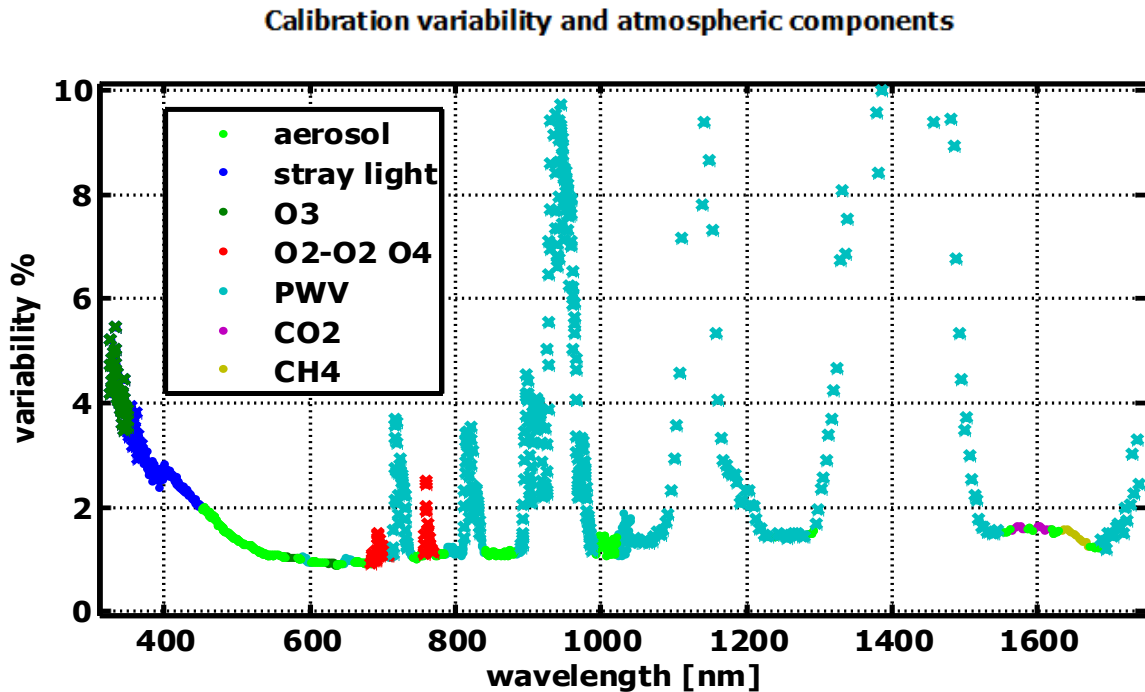


Figure 4. Retrieved  $I_o$  values for all pixels from the InGaAs linear array within the near-infrared (NIR) spectrometer design wavelength range. Note that many of these retrieved calibration values are invalid due to the effects of gas phase absorption especially by water vapor. The limited regions of applicability are discussed in Section 2.4.



**Figure 5.** Variability of the retrieved  $I_o$  values after interquartile filtering normalized to the mean and multiplied by 100 to convert to percent. The different color symbols represent different sources contributing to the variability of the  $I_o$  values. Increasing variability at wavelengths below 400 nm is due to a combination of reduced detector sensitivity, ozone absorption, and an uncorrected stray light artifact internal to the spectrometer. The numerous other “mountainous” features all represent absorption from different gas phase species. The “green valleys” represent regions where AOD may be confidently retrieved.

## 2.3 Obtaining Robust Daily Calibrations

Even after excluding cloud contaminated points from the Langley regressions and discarding the noisiest Langley regressions, the remaining “good”  $I_o$  values still exhibit a fairly high level of variability or random noise. This is visible in Figure 5 by the apparent “noise floor” of 1% or greater - even for presumably “good” wavelengths. It is also apparent in Figure 6 in the large variability observed in the collection of  $I_o$  values for 500 nm. Perhaps the most common cause of this random noise is subtle variation of the AOD during the time that the Langley regression takes place. Marengo (2007) demonstrates that a Langley regression can appear quite linear, and therefore apparently “good”, even when significant aerosol variation occurs. Fundamentally, any systematic variation in aerosol loading (decreasing or increasing) over the course of the Langley calibration will alter the slope of the regression line, thereby also altering the point where the regression line intercepts the y-axis at zero airmass (see Figure 1 again) leading to a substantial error in  $I_o$  and significant noise in a collection of derived  $I_o$  values. The practical solution applied in this VAP is to obtain a large enough collection of “good” Langley  $I_o$  values, extending several weeks both before and after the date of interest, and then filter these data to reduce the effect of noise sources discussed above.

Referring to Figure 6, let's now look at a time series of good  $I_o$  values. This particular time series is accumulated from about a year's time span using data from the ARM TCAP site on Cape Cod, Massachusetts (<http://campaign.arm.gov/tcap/>). The Langley retrieved  $I_o$  values are indicated by the blue circles. Over the time span considered here, 165 Langley retrievals were deemed good. All the  $I_o$  values illustrated in Figure 6 have been corrected for the eccentricity of the earth's orbit that occurs during the course of a year. This orbital variation results in measured irradiance variations of about  $\pm 3\%$ , and if left uncorrected this variation would show up as a "sine wave" in these data with a period of exactly one year, peaking in the January when the earth is closest to the sun, and the opposite six months later.

Figure 6 illustrates two important points. First, there are gaps during which the instrument was not producing data; for example, just prior to the beginning of 2013. Note that two calibration curves are necessary, one prior to the data gap and one after. Second, there is considerable noise in the  $I_o$  values of about  $\pm 20\%$ , even when only considering the "good" Langley events. This noise must be filtered out. Filtered smoothed "correct"  $I_o$  values for each day of the year are indicated by the red curves in Figure 6. Henceforth, we shall refer to the filtered smoothed  $I_o$  values as  $I_{o,f}$ . To calculate  $I_{o,f}$  values we follow a method described by Forgan (1988, 1994) and Chen et al. (2013).

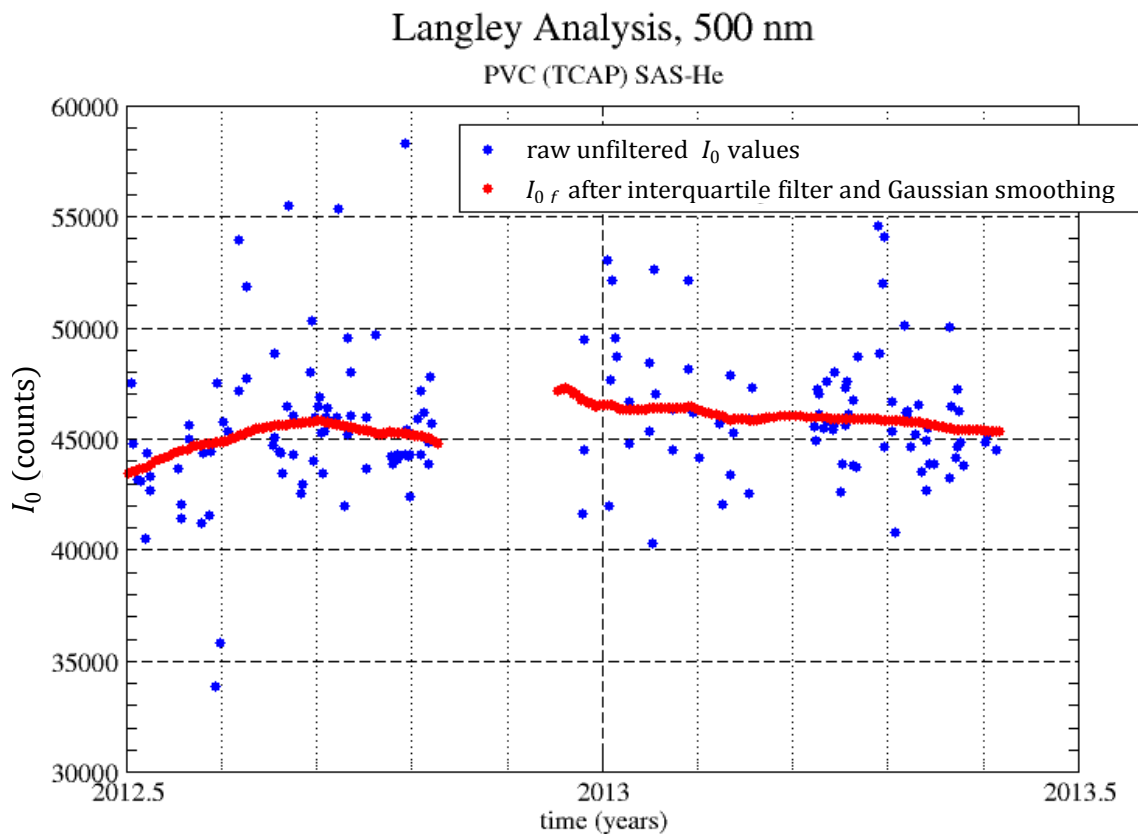


**Figure 6.** Time series of  $I_o$  values (blue dots) from the SAS-He at the ARM PVC site. The red curve segments are the corrected  $I_{o,f}$  resulting after applying a weighted average to  $I_o$  values within a  $\pm 5$  week sliding window to which an interquartile filter was first applied.

The filtering technique consists of a two-step process. The first is to apply an interquartile filter to a sliding window of full width 10 weeks to the  $I_o$  time series. Stepping along one day at a time, we consider all  $I_o$  values (for 550 nm and 673 nm) within the window and we remove all values in the lower and upper 25% quartiles. The underlying assumption here is that this pruning of points acts as a filter, eliminating outliers; we are then left with a time series of  $I_o$  values with considerably less noise. As a second step we compute  $I_{o,f}$  for the day at the center of the sliding window as a doubly-weighted average of the remaining  $I_o$  values. They are weighted in inverse proportion to the standard of deviation of the respective Langley regression ( $I_o$  values from weak regressions receive less weight) and are also weighted with a 36.5 day full width half maximum Gaussian envelope centered on the given day ( $I_o$  values from nearby Langley retrievals receive more weight than values separated by more time). The resulting filtered and smoothed  $I_{o,f}$  values vary slowly, typically showing much less than 1% variation per day as illustrated by the red curves in Figure 6. This process provides daily  $I_{o,f}$  values for any time of interest, except close to the times when the instrument hardware is changed, or the instrument is not operational for a significant period of time—a special situation discussed in Section 3.1.

## 2.4 Computing Total and Aerosol Optical Depths

With daily  $I_{o,f}$  values in hand, it is a trivial matter to calculate total optical depths (TODs) by rearranging Equation 4 to become

$$TOD(t) = (\tau_{Rayleigh} + \tau_{aerosol} + \tau_{gas}) = -\frac{1}{am} \ln \left[ \frac{I(\lambda, t)}{I_{o,f}(\lambda)} \right] \quad (5)$$

We note three things about this seemingly simple equation. First, we can calculate TOD during any time of the day during which the sun is up, provided that the following three conditions are met: first, we have a daily  $I_{o,f}$  value for that day, *and* there are no clouds between the SAS-He and the sun. Second, the gaseous absorption optical depth,  $\tau_{gas}$ , must be a linear function of airmass, or  $\tau_{gas}$  must be negligible, or else Equation 5 is not valid. And third, there is no requirement of an external irradiance calibration. The quantities  $I$  and  $I_{o,f}$  may be left in arbitrary units as their units will cancel reflecting that this process represents self-calibration in terms of the atmospheric transmittance.

Removal of the Rayleigh optical depth is trivial. Given the surface pressure, determining  $\tau_{Rayleigh}$  is found using the formula (Hansen and Travis, 1974):

$$\tau_{Rayleigh} = \frac{p}{1013.25} 0.008569\lambda^{-4} (1 + 0.0133\lambda^{-2} + 0.00013\lambda^{-4}) \quad (6)$$

where  $p$  is the surface pressure in millibars.

Accounting for the effects of gaseous absorption,  $\tau_{gas}$ , can be much more difficult. Generally speaking, water vapor, oxygen, CH<sub>4</sub>, and CO<sub>2</sub> exhibit nonlinear absorption with respect to airmass, and in many of these absorption regions, we cannot find the AOD, as illustrated in Figure 7 and Figure 8. These figures show TOD spectra, in which the Rayleigh optical depth has been removed, but the AOD and gaseous absorption remain. We first concentrate on the visible and near-IR range in Figure 7, obtained from the

“visible” spectrometer of the SAS-He. From about 400 to 450 nm, no gaseous absorption exists except for  $\text{NO}_2$ . The  $\text{NO}_2$  absorption is usually very small and can be neglected (although future versions of the VAP may try to account for its presence). Thus, the AOD spectrum in the spectral range, 400 to 450 nm, is the actual AOD. However, from about 450 nm and 750 nm, ozone absorption in the Chappuis band (Goody and Yung, 1989) is important. Some water vapor absorption also occurs in this spectral range. At places where vapor absorption is minimal, such as 500, 615, and 673 nm, the ozone absorption can be accounted for, and subtracted from the TOD. We denote the ozone gaseous absorption optical depth as  $\tau_{\text{ozone}}$ . (Note also that ozone absorbs solar radiation below about 350 nm. We will not discuss these absorption bands here.) Figure 7 also indicates other regions of the spectrum where gaseous absorption is negligible and AODs may be found. The spectral reach of these regions are small, and occur around 778 and 870 nm.

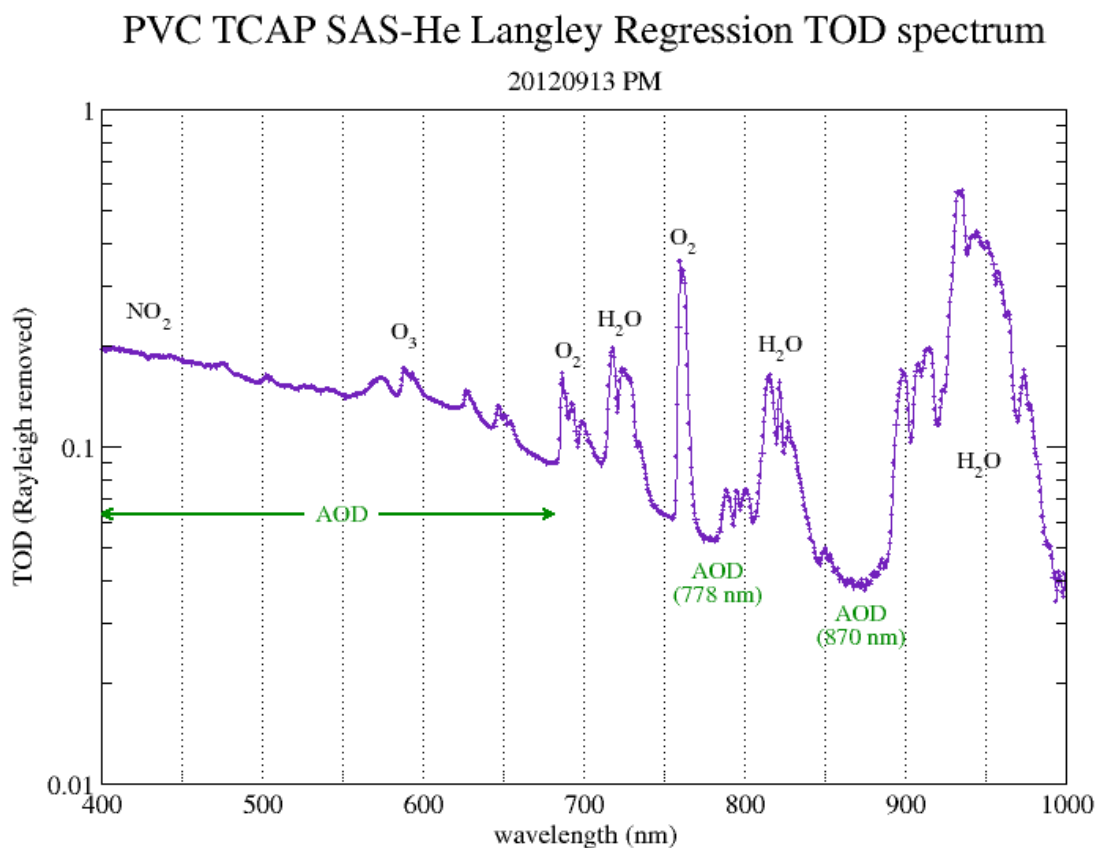


**Figure 7.** TOD spectrum with the Rayleigh component removed. The green markings indicate approximate spectral regions where the AOD may be effectively retrieved. Gaseous absorption regions are indicated by the species that is responsible for the absorption; however, for the sake of clarity, some minor absorption regions are omitted. AODs may be found from about 400 to 675 nm (if care is taken to avoid regions of water vapor absorption), and over short wavelength segments centered on 778 and 870 nm. Figure 2 in Dunagan et al. (2013) shows a more detailed view of the gaseous absorption.

Finding the ozone optical depth is straightforward, if we have an estimate of the columnar amount of ozone. For this value, we use data from the TOMS (Total Ozone Mapping Spectrometer; <http://toms.gsfc.nasa.gov>) satellite, or the OMI (Ozone Monitoring Instrument (<http://aura.gsfc.nasa.gov/instruments/omi.html>)), which has been stored in the ARM Data Archive

from 1996/07/25 to the present time. (In the Archive, the data stream is named *gecomiX1.a1*). Using the latitude and longitude at which the SAS-He is physically located, we determine a suitable ozone value by an interpolation technique. If no ozone data is available for a particular day, a site specific default value is used. Once we have a columnar value of ozone (with the rather arcane units of “atmosphere-centimeter” [atm-cm], which are equal to one Dobson Unit divided by 1000, <http://ozonewatch.gsfc.nasa.gov/>), we find  $\tau_{ozone}$  as

$$\tau_{ozone}(\lambda) = (\text{Columnar ozone, atm.cm}) * A_{ozone}(\lambda) \quad (7)$$

where “Columnar ozone, atm-cm” is the amount of ozone in the atmospheric column, and  $A_{ozone}(\lambda)$  is the ozone gas absorption coefficient – a function of wavelength. For the Chappuis band, the absorption coefficients are listed in Appendix 1.

Figure 8 shows a figure analogous to Figure 7, for the SAS-He “near-IR” spectrometer. Note that for most spectral regions the gaseous absorption is quite large, precluding the easy inference of an AOD. There are, however, several spectral areas with minimal gaseous absorption, and for these areas, gaseous absorption can be accounted for. These areas are found around 1020, 1250, and 1623 nm. (Other regions exist but are not shown here – see Figure 2 in Dunagan et al. [2013]).

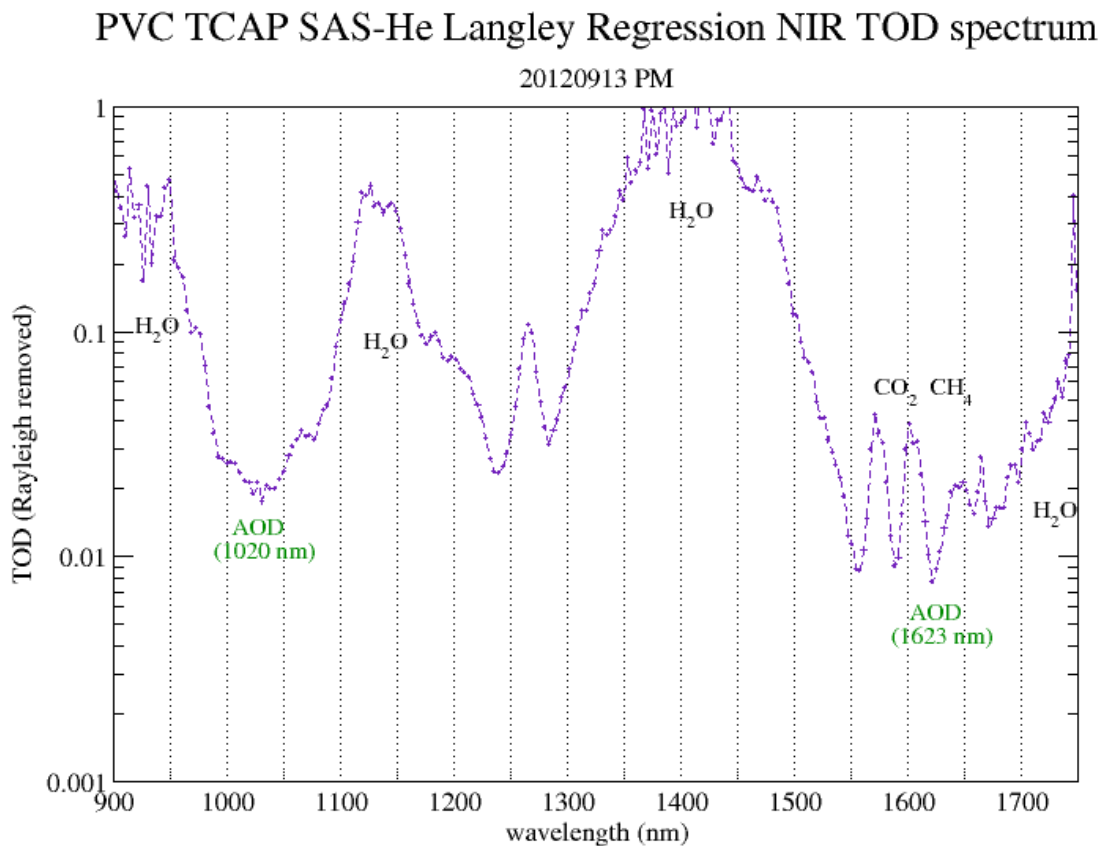


**Figure 8.** Same as Figure 7 except for the near-IR region extending from about 900 to 1750 nm. See Figure 2 in Dunagan et al. (2013) for a more detailed view of the gaseous absorption.

Two wavelengths regions indicated in Figure 8, at which AODs may be found, require slight corrections because of absorption by water vapor (1020 nm), and water vapor, CO<sub>2</sub>, and CH<sub>4</sub> (1623 nm). The suggested corrections are listed in Table 1. **These corrections are not (yet) applied in the netcdf files.** However, plans are afoot to develop additional correction expressions for other spectral wavelengths, and to apply both the new and the Table 1 expressions to correct significant portions of the entire SAS-He spectrum for gaseous absorption.

**Table 1.** Corrections for gaseous absorption for two selected wavelengths in the near-IR. The abbreviation “pwv” stands for precipitable water vapor, with units cm. The 1020 nm correction is from the AERONET program (<http://aeronet.gsfc.nasa.gov/>), while the 1623 nm correction is from Joe Michalsky (private communication, 2013).

Wavelength	Water vapor (pwv) correction	CH <sub>4</sub> correction (sea level)	CO <sub>2</sub> correction (sea level)
1020 nm	$0.0023 * pwv + 0.0002$	-	-
1623 nm	$0.0051 * (pwv/5)^{1/2}$	0.0031	0.007

At the present, the above corrections are the only corrections available.

## 2.5 Aerosol Optical Depths – An Example

Figure 9 shows a typical AOD time series obtained from the SAS-He at the ARM PVC site, for the date April 1, 2013. The AODs are shown for a single wavelength of 500 nm, but again be aware that AODs can be found for a wide range of wavelengths because of the spectral nature of the SAS-He. The AODs for this particular day are quite low; for 500 nm the average AOD is about 0.04. The estimated error of AODs obtained from the technique described above is  $\pm 0.01$ . However, some of the plotted AODs are contaminated by cloud and need to be removed; see, for example, the data prior to about 0800 hours and after about 1600 hours, local standard time (LST). This removal will be discussed below.

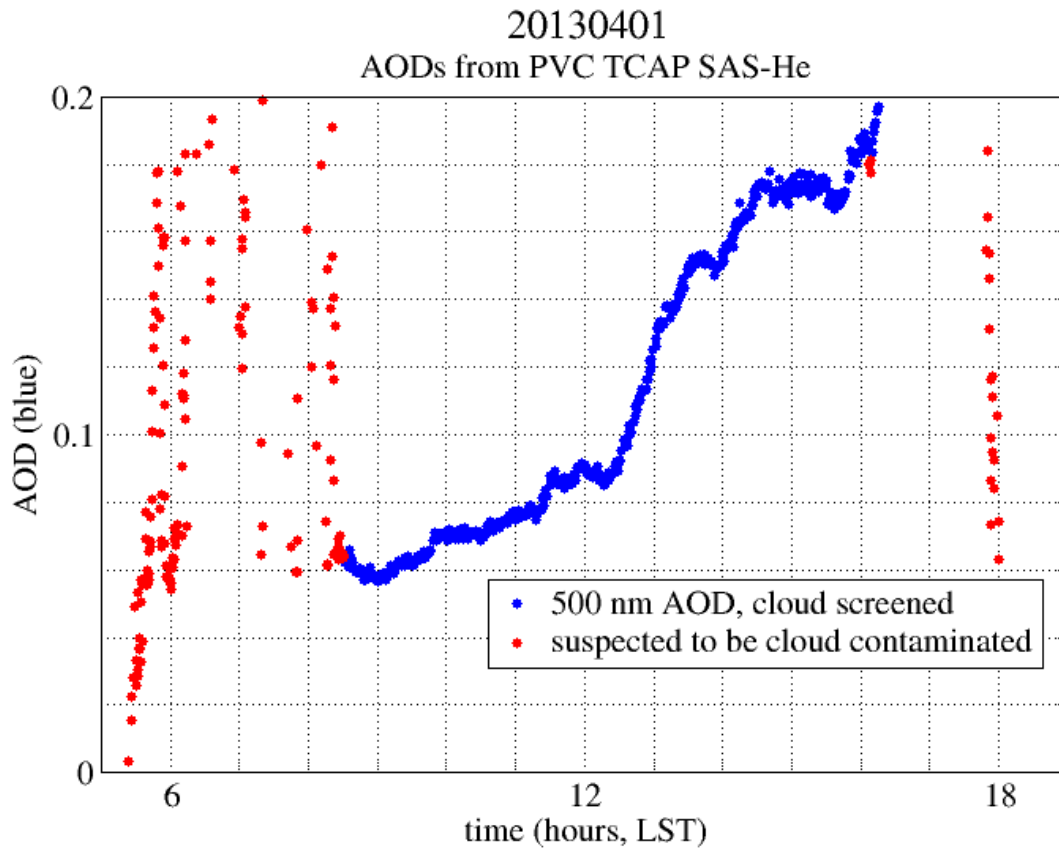


**Figure 9.** Time series of AOD for 500 nm wavelength for April 1, 2013 at the ARM PVC site. The blue dots indicate AODs that are not contaminated by clouds or other factors. The red dots show points that are deemed “contaminated” after a cloud screen has been applied.

## 2.6 Application of a Cloud Screen

In Figure 9, cloud contamination of AOD is evident at times such as the early morning hours when the AOD is highly variable over short periods of time (10 minutes). We remove these erroneous AODs from the time series through a procedure we call “cloud screening”. This screening is based on the algorithm of Alexandrov et al. (2004). Briefly, this algorithm examines the variability of an AOD time series. If the variability is small over a specified time interval, the AODs are assumed to be good. Otherwise they are rejected. The demarcation between accepted and rejected AODs is a specified parameter—the so-called “threshold value”—and it is determined by both quantitative as well as visual analysis. The parameter is adjusted to be conservative; that is, it tends to identify some AODs as being contaminated, when in fact they are not, thereby embracing the philosophy that it is better to error on the side of removing a few good AODs rather than letting a significant number of cloud contaminated AODs slip through. Threshold values used in the VAP were derived following the procedures described in Kassianov et al. (2013). Figure 9 shows the cloud screen applied to the AODs. The blue dots in this are the AODs that have been screened, and deemed acceptable, whereas the red dots show “AODs” that are likely to be cloud contaminated. For additional cloud screening considerations, see Kassianov et al. (2013).

## 3.0 Algorithm Technical Considerations

### 3.1 Change of Hardware or Unexpected Data Gaps

At the time of an SAS-He hardware change (or if the instrument is down for a significant amount of time) a discontinuity is introduced into the calibration process. In the case of a hardware change, this discontinuity stems from the fact that the nominal calibration of the SAS-He differs between instruments, therefore causing an abrupt step up, or step down, in  $I_o$  values precisely at the time that the hardware change takes place. The sliding window method, described above, cannot be applied over the boundaries where this step change occurs. In these situations one edge of the sliding window, of width about 60 days, is allowed to butt up against the step change, and the smoothed value at the middle of window is used as the  $I_o$  value from this middle point to the time of the calibration change. This procedure is also employed when a significant gap exists in the data, perhaps caused by an instrument malfunction, extended power outages, etc.

### 3.2 VAP Output

The output from the SAS-He Langley and SAS-He AOD VAPs are daily netCDF files named according to standard ARM conventions. For example,

```
pvcsashevislangleyM1.c1.20130529.091004.cdf,
```

and

```
pvcsashevisaodM1.c1.20130529.091004.cdf,
```

contain output of the Langley VAP and AOD VAP, respectively, at the PVC M1 site on May 29, 2013. Refer to Appendix B for the structure of these netCDF files.

### 3.3 Running the SAS-He Langley and AOD VAPs (command line arguments)

Typical command lines, with options, for the SAS-He Langley and AOD VAPs, are:

```
sashe_langley -s sss -f Fn -b begin_date -e end_date
```

```
sashe_aod -s sss -f Fn -b begin_date -e end_date
```

with arguments:

```
-s sss - Specifies the three character site identifier, such as
```

```
“sgp” for Southern Great Plains,
```

```
“pvc” for Cape Cod, Massachusetts
```

- f Fn - Specifies the facility identifier, such as “C1” or “M1”
- b YYYYMMDD - Specifies the begin date in the form YYYYMMDD.  
Data starting from and including this date will be processed.
- e YYYYMMDD - Specifies the end date in the form YYYYMMDD.  
Data will be processed up to but \*NOT\* including this date.

and options:

- a alias - Specify the .db\_connect alias to use (default: dsdb\_data).
- h - Display help message.
- v - Display VAP version.
- D [level] - Turn on debug mode.
- P [level] - Turn on provenance logging.
- R - Enable reprocessing/development mode. Enabling this mode  
will allow previously processed data to be overwritten.

For normal operations the SAS-He Langley process is run daily for the previous day. The SAS-He AOD process must be run with at least a 5 week lag and requires that OMI ozone data (i.e. gecomiX1.a1) exists for the day that it is run for. The OMI data comes in monthly with a two week lag at the end of the month. This will typically result in a 6 week lag before the SAS-He AOD process can be run.

### 3.4 Data Quality Assessment Included

The datastream contains essentially all the auxiliary fields which relate to the determination of the instrument calibration and computation of AOD, and quality-check “qc” fields exist for many of them. But most importantly, the primary measured quantities of direct normal transmittance, diffuse hemispheric transmittance, and AOD each contain detailed qc fields which report the results of pass/fail tests and assessments of the corresponding impact on the data values. The ARM convention is to report failed QC tests as non-zero values. The most conservative use of these fields would be to use only those measurement values when the corresponding “qc” fields are zero. However, not all of these QC tests carry equal weight. Some flags indicate conditions of potential concern or indeterminate results while others indicate more damning conditions. The data user is advised to carefully examine the various QC values and the underlying reasons for a particular QC bit being set. By ARM convention, QC bit information is available via variable attributes in the output netcdf files.

### 3.5 Known Issues

The SAS-He instruments are relatively new as are the data processing modules described here. There are a number of known issues that have not been fully resolved. Some of these represent known processing steps that have merely been postponed pending the release of this initial product, while others represent incompletely understood instrument issues. These issues are briefly described below along with general descriptions of the expected impact. As with all new instruments, it is likely that there are other as yet unidentified issues.

1. **Uncorrected ozone absorption below 350 nm.** Although we account for the ozone Chappuis absorption band around 600 nm (which is fairly linear) we do not yet account for the Huggins bands between 320-360 nm. AODs estimated with the correction will be slightly lower than those estimated without the correction.
2. **Stray light contamination below 400 nm.** We have an unresolved hardware issue with stray light that impacts wavelengths less than about 400 nm. This effect varies with time of day and is most severe when the sun is low or deeply attenuated due to the reduced ambient UV irradiances. The impact is evident as a reduction in AOD at short wavelengths at low sun angles.
3. **Gas phase corrections in the near infrared (NIR) region not applied.** As described in Section 2.4 and shown in Table 1, the AOD values reported from the NIR spectrometer have not been corrected for contributions from water vapor, methane, and carbon dioxide. We have suggested corrections at discrete wavelengths of 1020 and 1623 nm but do not yet have corrections as a continuous function of pixel or wavelength. However, such work is planned in the near future. AODs with the correction will be slightly lower than those without the correction.
4. **Uncertain Langley  $I_0$  values in vicinity of gaseous absorption features.** Beyond merely making it difficult to deduce the AOD at wavelengths where significant gaseous absorption occurs, uncertainties in Langley  $I_0$  values in these regions may affect the calibration itself, leading to larger uncertainties in the solar irradiance estimates. We caution the user to avoid when possible these spectral regions, or else to use them with extreme care.

## 4.0 References

- Alexandrov, M, A Marshak, B Cairns, A Lacis, and B Carlson. 2004. "Automated cloud screening algorithm for MFRSR data." *Geophysical Research Letters* 31: L04118, doi:10.1029/2003GL019105.
- Chen, M., J Davis, T Hongzhao, C Ownby, and G Wei. 2013. "The calibration methods for multi-filter rotating shadowband radiometer: A review." *Frontiers of Earth Science* 7(3): 257–270, doi: 10.1007/s11707-013-0368-9, 2013.
- Dunagan, SE, R Johnson, J Zavaleta, PB Russell, B Schmid, C Flynn, J Redemann, Y Shinozuka, J Livingston, and M Segal-Rosenhaimer. 2013. "4STAR spectrometer for sky-scanning sun-tracking atmospheric research: Instrument technology." *Remote Sensing* 5(8): 3872-3895, doi:10.3390/rs5083872.
- Forgan, BW. 1986. "Sun photometer calibration by the ratio-Langley method." In *Baseline Atmospheric Program (Australia)* edited by BW Forgan and PJ Fraser, Bureau of Meteorology, Melbourne, Australia, 1988, pp. 22-26.
- Forgan, BW. 1994. "General method for calibrating Sun photometers." *Applied Optics* 33(21): 4841-4850.
- Goody, RM and YL Yung. 1989. *Atmospheric Radiation. Theoretical Basis*. New York, Oxford University Press.
- Gueymard, CA. 2004. "The Sun's total and spectral irradiance for solar energy applications and solar radiation models." *Solar Energy* 76(4): 423-453.
- Hansen, J and L Travis. 1974. "Light scattering in planetary atmospheres." *Space Science Reviews* 16: 527-610.
- Harrison, L and J Michalsky. 1994. "Objective algorithms for the retrieval of optical depths from ground-based measurements." *Applied Optics* 33: 5126-5132.
- Kassianov, E, C Flynn, A Koontz, C Sivaraman, and J Barnard. 2013. "Failure and redemption of MFRSR/NIMFR cloud screening: Contrasting algorithm performance at ARM NSA and SGP sites." *Atmosphere* 4: 299-314, doi:10.3390/atmos4030299.
- Kasten, F and A Young. 1989. "Revised optical air mass tables and approximation formula." *Applied Optics* 28: 4735-4738.
- Kiedron, P, J Michalsky, J Berndt, and L Harrison. 1999. "A comparison of spectral irradiance standards used to calibrate shortwave radiometers and spectroradiometers." *Applied Optics* 38(12): 2432-2439.
- Koontz, A, C Flynn, G Hodges, J Michalsky, and J Barnard. 2013. "Aerosol Optical Depth Value-Added Product." U.S. Department of Energy. DOE/SC-ARM/TR-129.

Marengo, F. 2007. "On Langley plots in the presence of a systematic diurnal aerosol cycle centered at noon: A comment on recently proposed methodologies." *Journal of Geophysical Research* 112: D06205, doi:10.1029/2006JD007248.

Michalsky, JJ, J Schlemmer, W Berkheiser, J Berndt, L Harrison, N Laulainen, N Larson, and J Barnard. 2001. "Multiyear measurements of aerosol optical depth in the Atmospheric Radiation Measurement and Quantitative Links programs." *Journal of Geophysical Research* 106(D11): 12099-12107.

Schmid, B and C Wehrli. 1995. "Comparison of Sun photometer calibration by use of the Langley technique and the standard lamp." *Applied Optics* 34(21): 4500-4512.

Schmid, B, JJ Michalsky, DW Slater, JC Barnard, RN Halthore, JC Liljegren, BN Holben, TF Eck, JM Livingston, PB Russell, T Ingold, and I Slutsker. 2001. "Comparison of columnar water-vapor measurements from solar transmittance methods." *Applied Optics* 40(12): 1886-1896.

## Appendix A

### Table of wavelength versus ozone absorption coefficients

Multiply the appropriate coefficient by the columnar amount of ozone in atm-cm to find the ozone optical depth,  $\tau_{ozone}$ . Note that one atm-cm is equal to DU/1000; recall that DU stands for Dobson Unit. For example, for a columnar amount of ozone of 300 DU, at 615 nm,  $\tau_{ozone} = 300/1000 * 0.1162 = 0.03486$ .

Table 2.

$\lambda$	Ozone Absorption Coefficient								
380	0.0000	381	0.0000	382	0.0000	383	0.0000	384	0.0000
385	0.0000	386	0.0000	387	0.0000	388	0.0000	389	0.0000
390	0.0000	391	0.0000	392	0.0000	393	0.0000	394	0.0000
395	0.0000	396	0.0000	397	0.0000	398	0.0000	399	0.0000
400	0.0000	401	0.0000	402	0.0000	403	0.0000	404	0.0000
405	0.0000	406	0.0000	407	0.0001	408	0.0002	409	0.0002
410	0.0003	411	0.0003	412	0.0003	413	0.0003	414	0.0003
415	0.0003	416	0.0004	417	0.0005	418	0.0005	419	0.0005
420	0.0005	421	0.0006	422	0.0007	423	0.0008	424	0.0010
425	0.0012	426	0.0013	427	0.0013	428	0.0013	429	0.0012
430	0.0012	431	0.0013	432	0.0015	433	0.0017	434	0.0017
435	0.0017	436	0.0017	437	0.0018	438	0.0021	439	0.0024
440	0.0029	441	0.0033	442	0.0037	443	0.0039	444	0.0040
445	0.0038	446	0.0036	447	0.0035	448	0.0035	449	0.0038
450	0.0042	451	0.0045	452	0.0046	453	0.0046	454	0.0046
455	0.0047	456	0.0052	457	0.0059	458	0.0069	459	0.0078
460	0.0087	461	0.0095	462	0.0098	463	0.0097	464	0.0092
465	0.0087	466	0.0084	467	0.0086	468	0.0092	469	0.0096
470	0.0101	471	0.0104	472	0.0105	473	0.0105	474	0.0108
475	0.0115	476	0.0127	477	0.0141	478	0.0158	479	0.0174
480	0.0193	481	0.0206	482	0.0215	483	0.0218	484	0.0213
485	0.0205	486	0.0200	487	0.0196	488	0.0197	489	0.0203
490	0.0213	491	0.0219	492	0.0223	493	0.0225	494	0.0230
495	0.0234	496	0.0244	497	0.0257	498	0.0274	499	0.0295
500	0.0320	501	0.0346	502	0.0372	503	0.0396	504	0.0414
505	0.0427	506	0.0431	507	0.0429	508	0.0423	509	0.0415
510	0.0409	511	0.0405	512	0.0410	513	0.0418	514	0.0428
515	0.0437	516	0.0446	517	0.0455	518	0.0463	519	0.0471
520	0.0481	521	0.0496	522	0.0511	523	0.0531	524	0.0554
525	0.0580	526	0.0605	527	0.0633	528	0.0659	529	0.0684
530	0.0706	531	0.0725	532	0.0740	533	0.0749	534	0.0754
535	0.0755	536	0.0753	537	0.0753	538	0.0757	539	0.0764
540	0.0774	541	0.0787	542	0.0803	543	0.0819	544	0.0833

$\lambda$	Ozone Absorption Coefficient								
545	0.0846	546	0.0856	547	0.0866	548	0.0875	549	0.0882
550	0.0890	551	0.0899	552	0.0908	553	0.0918	554	0.0931
555	0.0944	556	0.0962	557	0.0981	558	0.1002	559	0.1027
560	0.1052	561	0.1078	562	0.1104	563	0.1128	564	0.1148
565	0.1166	566	0.1184	567	0.1199	568	0.1213	569	0.1229
570	0.1244	571	0.1257	572	0.1268	573	0.1275	574	0.1279
575	0.1278	576	0.1273	577	0.1264	578	0.1254	579	0.1243
580	0.1231	581	0.1219	582	0.1208	583	0.1197	584	0.1190
585	0.1184	586	0.1180	587	0.1179	588	0.1178	589	0.1180
590	0.1185	591	0.1196	592	0.1208	593	0.1226	594	0.1248
595	0.1270	596	0.1295	597	0.1318	598	0.1341	599	0.1360
600	0.1375	601	0.1384	602	0.1390	603	0.1388	604	0.1382
605	0.1371	606	0.1356	607	0.1337	608	0.1317	609	0.1294
610	0.1271	611	0.1248	612	0.1224	613	0.1203	614	0.1181
615	0.1162	616	0.1142	617	0.1124	618	0.1108	619	0.1092
620	0.1078	621	0.1065	622	0.1052	623	0.1039	624	0.1027
625	0.1014	626	0.1000	627	0.0987	628	0.0973	629	0.0957
630	0.0943	631	0.0929	632	0.0916	633	0.0901	634	0.0886
635	0.0870	636	0.0855	637	0.0839	638	0.0823	639	0.0807
640	0.0790	641	0.0775	642	0.0761	643	0.0747	644	0.0734
645	0.0720	646	0.0708	647	0.0696	648	0.0683	649	0.0673
650	0.0662	651	0.0652	652	0.0641	653	0.0630	654	0.0619
655	0.0608	656	0.0597	657	0.0586	658	0.0575	659	0.0565
660	0.0555	661	0.0546	662	0.0536	663	0.0526	664	0.0516
665	0.0505	666	0.0494	667	0.0482	668	0.0471	669	0.0460
670	0.0450	671	0.0440	672	0.0429	673	0.0419	674	0.0409
675	0.0401	676	0.0392	677	0.0383	678	0.0375	679	0.0368
680	0.0361	681	0.0355	682	0.0350	683	0.0345	684	0.0339
685	0.0333	686	0.0327	687	0.0320	688	0.0311	689	0.0303
690	0.0295	691	0.0287	692	0.0279	693	0.0273	694	0.0265
695	0.0258	696	0.0251	697	0.0244	698	0.0237	699	0.0232
700	0.0226	701	0.0221	702	0.0217	703	0.0212	704	0.0208
705	0.0205	706	0.0202	707	0.0199	708	0.0196	709	0.0193
710	0.0191	711	0.0189	712	0.0187	713	0.0185	714	0.0185
715	0.0183	716	0.0181	717	0.0177	718	0.0173	719	0.0168
720	0.0162	721	0.0156	722	0.0151	723	0.0147	724	0.0143
725	0.0140	726	0.0136	727	0.0134	728	0.0130	729	0.0126
730	0.0123	731	0.0120	732	0.0118	733	0.0116	734	0.0115
735	0.0114	736	0.0114	737	0.0113	738	0.0112	739	0.0112
740	0.0112	741	0.0113	742	0.0115	743	0.0116	744	0.0117
745	0.0118	746	0.0120	747	0.0119	748	0.0118	749	0.0116

$\lambda$	Ozone Absorption Coefficient								
750	0.0111	751	0.0106	752	0.0101	753	0.0096	754	0.0090
755	0.0086	756	0.0082	757	0.0079	758	0.0077	759	0.0075
760	0.0073	761	0.0072	762	0.0070	763	0.0070	764	0.0070
765	0.0069	766	0.0068	767	0.0067	768	0.0067	769	0.0068
770	0.0068	771	0.0069	772	0.0071	773	0.0072	774	0.0075
775	0.0079	776	0.0081	777	0.0083	778	0.0084	779	0.0085
780	0.0084	781	0.0082	782	0.0079	783	0.0075	784	0.0071
785	0.0067	786	0.0063	787	0.0061	788	0.0058	789	0.0056
790	0.0054	791	0.0052	792	0.0049	793	0.0047	794	0.0046
795	0.0044	796	0.0043	797	0.0042	798	0.0042	799	0.0041
800	0.0040	801	0.0040	802	0.0040	803	0.0039	804	0.0040
805	0.0040	806	0.0041	807	0.0042	808	0.0044	809	0.0046
810	0.0048	811	0.0050	812	0.0052	813	0.0054	814	0.0056
815	0.0057	816	0.0057	817	0.0057	818	0.0056	819	0.0055
820	0.0052	821	0.0049	822	0.0046	823	0.0043	824	0.0040
825	0.0037	826	0.0034	827	0.0031	828	0.0029	829	0.0027
830	0.0025	831	0.0024	832	0.0023	833	0.0022	834	0.0021
835	0.0021	836	0.0020	837	0.0020	838	0.0020	839	0.0020
840	0.0020	841	0.0020	842	0.0021	843	0.0021	844	0.0022
845	0.0023	846	0.0024	847	0.0026	848	0.0028	849	0.0030
850	0.0032	851	0.0035	852	0.0037	853	0.0038	854	0.0038
855	0.0037	856	0.0036	857	0.0035	858	0.0033	859	0.0032
860	0.0029	861	0.0027	862	0.0025	863	0.0023	864	0.0021
865	0.0019	866	0.0017	867	0.0016	868	0.0015	869	0.0014
870	0.0013	871	0.0013	872	0.0012	873	0.0011	874	0.0011
875	0.0011	876	0.0010	877	0.0010	878	0.0010	879	0.0010
880	0.0011	881	0.0011	882	0.0011	883	0.0011	884	0.0012
885	0.0012	886	0.0013	887	0.0013	888	0.0013	889	0.0014
890	0.0014	891	0.0013	892	0.0013	893	0.0014	894	0.0014
895	0.0015	896	0.0016	897	0.0016	898	0.0017	899	0.0017
900	0.0016	901	0.0015	902	0.0014	903	0.0014	904	0.0013
905	0.0012	906	0.0011	907	0.0010	908	0.0009	909	0.0009
910	0.0008	911	0.0007	912	0.0007	913	0.0006	914	0.0006
915	0.0005	916	0.0005	917	0.0005	918	0.0005	919	0.0005
920	0.0005	921	0.0004	922	0.0004	923	0.0004	924	0.0004
925	0.0004	926	0.0004	927	0.0004	928	0.0004	929	0.0004
930	0.0004	931	0.0004	932	0.0004	933	0.0004	934	0.0004
935	0.0005	936	0.0005	937	0.0005	938	0.0006	939	0.0007
940	0.0008	941	0.0009	942	0.0010	943	0.0011	944	0.0011
945	0.0011	946	0.0010	947	0.0009	948	0.0008	949	0.0007
950	0.0007	951	0.0006	952	0.0005	953	0.0005	954	0.0004

$\lambda$	Ozone Absorption Coefficient								
955	0.0004	956	0.0004	957	0.0004	958	0.0003	959	0.0003
960	0.0003	961	0.0000	962	0.0000	963	0.0000	964	0.0000
965	0.0000	966	0.0000	967	0.0000	968	0.0000	969	0.0000
970	0.0000	971	0.0000	972	0.0000	973	0.0000	974	0.0000
975	0.0000								

## Appendix B

### Contents of netCDF output for the SAS-He Langley VAP

In the ARM Data Archive, these files are given names such as  
 “pvcashevislangleyM1.c1.20130529.091004.cdf”

**Table 3.**

<b>variable</b>	<b>dimensions</b>	<b>units</b>
base_time		seconds since 1970-1-1 0:00:00 0:00
time_offset	(time)	seconds since 2013-05-29 05:00:00 0:00
time	(time)	seconds since 2013-05-29 00:00:00 0:00
wavelength	(wavelength)	nm
solar_zenith_angle	(time)	deg
cosine_solar_zenith_angle	(time)	unitless
cosine_correction	(time)	unitless
airmass	(time)	unitless
airmass_mask	(time)	unitless
earth_sun_dist	(time)	AU
solar_spectrum	(wavelength)	W/(m <sup>2</sup> nm)
direct_normal_irradiance	(time, wavelength)	counts
direct_normal_irradiance_mask	(time, wavelength)	unitless
am_lo	(wavelength)	counts
am_lo_std	(wavelength)	counts
am_tau	(wavelength)	unitless
am_tau_std	(wavelength)	unitless
am_chi2	(wavelength)	unitless
pm_lo	(wavelength)	counts
pm_lo_std	(wavelength)	counts
pm_tau	(wavelength)	unitless
pm_tau_std	(wavelength)	unitless
pm_chi2	(wavelength)	unitless
lat		degree_N
lon		degree_E
alt		m

## Appendix C

### Contents of netCDF output for the SAS-He AOD VAP

In the ARM archive, these files are given names such as “pvcsashevisaodM1.c1.20130529.091004.cdf”

Table 4.

variable	dimensions	units
base_time		seconds since 1970-1-1 0:00:00 0:00
time_offset	(time)	seconds since 2013-05-29 05:00:00 0:00
time	(time)	seconds since 2013-05-29 00:00:00 0:00
wavelength	(wavelength)	nm
Io_time	(Io_time)	seconds since 2013-04-26 11:00:00 0:00
Io_values	(Io_time, wavelength)	counts
Io_values_std	(Io_time, wavelength)	counts
smoothed_Io_values	(wavelength)	counts
qc_smoothed_Io_value	(wavelength)	unitless
solar_zenith_angle	(time)	deg
cosine_solar_zenith_angle	(time)	unitless
cosine_correction	(time)	unitless
diffuse_correction		unitless
airmass	(time)	unitless
earth_sun_dist	(time)	AU
atmos_pressure	(time)	kPa
qc_atmos_pressure	(time)	unitless
rayleigh_optical_depth	(wavelength)	unitless
ozone_columnar_density		DU
ozone_absorption_coefficient	(wavelength)	1/cm
ozone_optical_depth	(wavelength)	unitless
solar_spectrum	(wavelength)	W/(m <sup>2</sup> nm)
diffuse_transmittance	(time, wavelength)	unitless
qc_diffuse_transmittance	(time, wavelength)	unitless
direct_normal_transmittance	(time, wavelength)	unitless
qc_direct_normal_transmittance	(time, wavelength)	unitless
normalized_atmospheric_variability	(time)	unitless
aerosol_optical_depth	(time, wavelength)	unitless
qc_aerosol_optical_depth	(time, wavelength)	unitless
lat		degree_N
lon		degree_E
alt		m



U.S. DEPARTMENT OF  
**ENERGY**

---

Office of Science